Supporting Information for

Effect of coordinated anions on ferromagnetically coupled Dy_2 zero-field single-molecule magnets

Cai-Ming Liu,*[a] Xiang Hao,[a] Dong-Mei Zhu*[b] and Yi-Quan Zhang[b]

[a] *Beijing National Laboratory for Molecular Sciences, CAS Key Laboratory for Organic Solids, Institute of Chemistry, Chinese Academy of Sciences, Beijing 100190, China. E-mail: cmliu@iccas.ac.cn*
[b] *Jiangsu Key Laboratory for NSLSCS, School of Physical Science and Technology, Nanjing Normal University, Nanjing 210023, China. E-mail: 221001007@njnu.edu.cn*

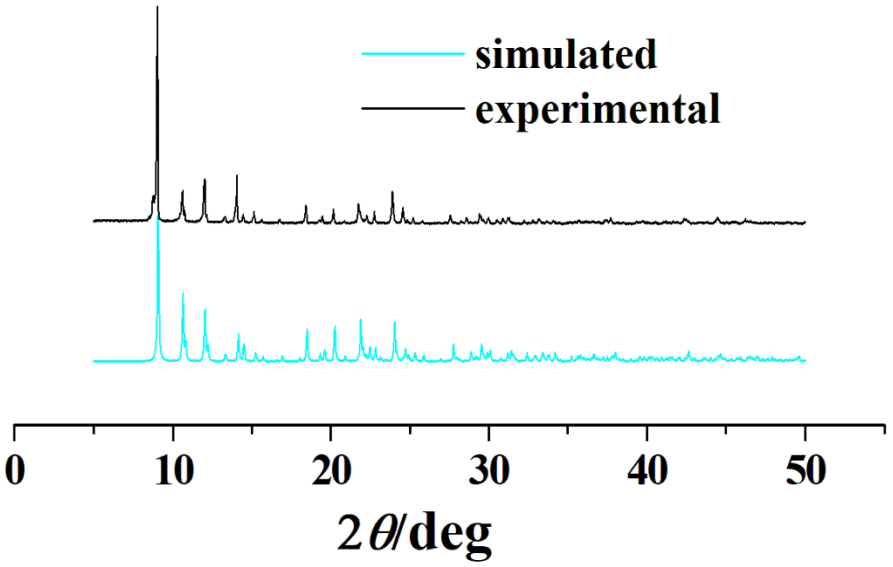

Fig. S1. The simulative and experimental powder X-ray diffraction patterns for **1**.

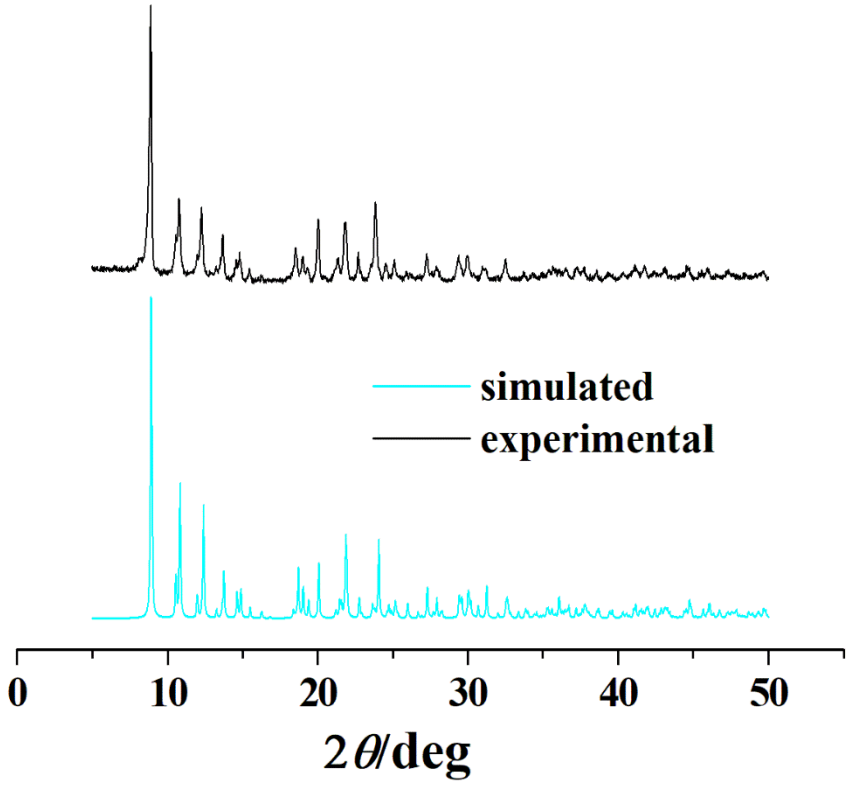

Fig. S2. The simulative and experimental powder X-ray diffraction patterns for **2**.

Table S1. Dy (III) ion geometry analysis by SHAPE 2.1 software for **1** and **2**.

Complex	**1**	**2**
Configuration	ABOXIY **Dy1**	ABOXIY **Dy1**
Octagon(D_{8h})	31.479	31.324
Heptagonal pyramid(C_{7v})	21.065	21.438
Cube (O_h)	15.285	15.371
Hexagonal bipyramid(D_{6h})	13.237	13.991
Square antiprism (D_{4d})	5.901	5.942
Triangular dodecahedron (D_{2d})	**3.495**	3.917
Johnson gyrobifastigium J26 (D_{2d})	11.369	11.438
Johnson elongated triangular bipyramid J14 (D_{3h})	23.067	22.734
Biaugmented trigonal prism J50 (C_{2v})	3.663	3.496
Biaugmented trigonal prism (C_{2v})	3.631	**3.325**
Snub diphenoid J84 (D_{2d})	4.267	4.807
Triakis tetrahedron (T_d)	13.924	14.620
Elongated trigonal bipyramid (D_{3h})	21.413	20.796

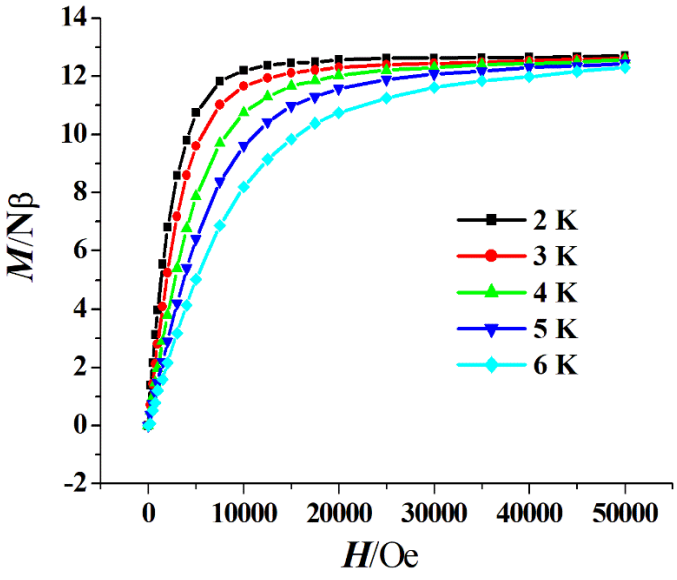

Fig. S3. *M versus H* plots at 2-6 K of **1**.

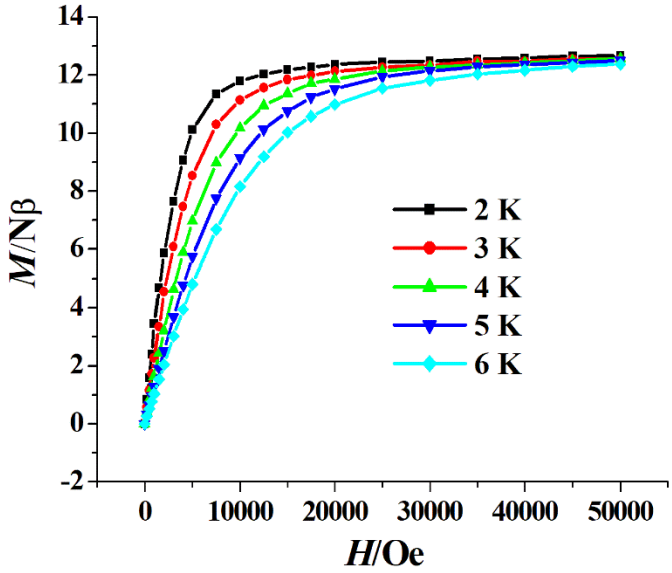

Fig. S4. *M versus H* plots at 2-6 K of **2**.

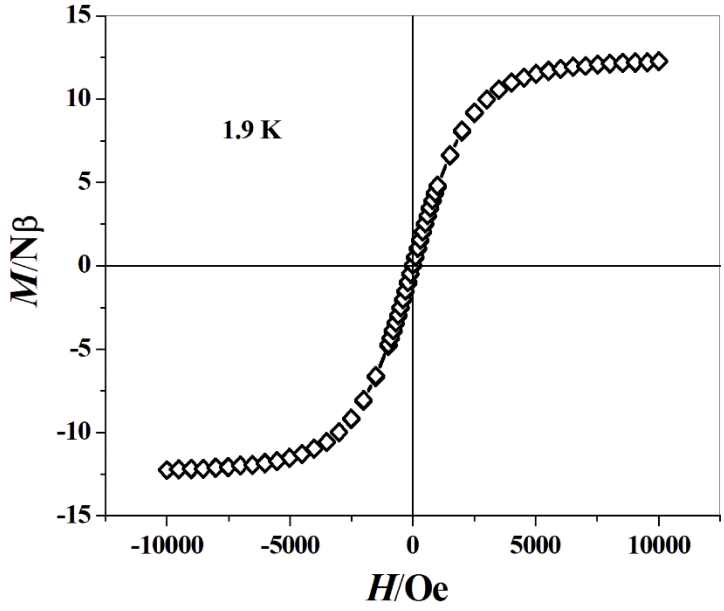

Fig. S5. Hysteresis loop for **1** at 1.9 K with the normal sweep rate (100-300 Oe min^{-1}).

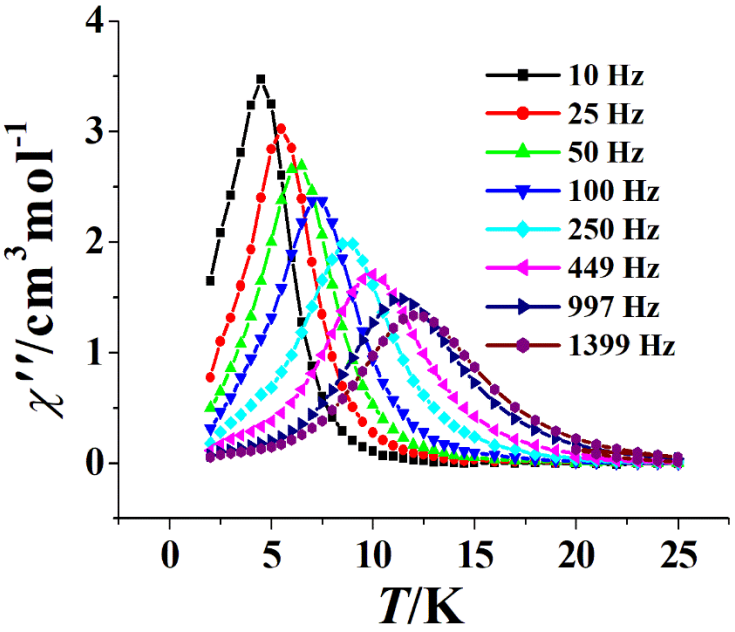

Fig. S6. Plots of χ'' *versus* T for **1** (H_{dc} = 1500 Oe).

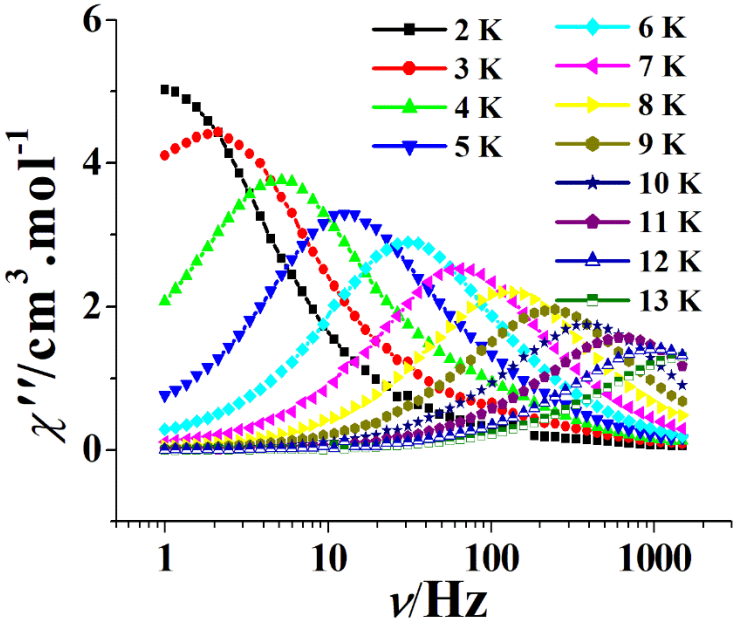

Fig. S7. Plots of χ'' *versus* ν for **1** (H_{dc} = 1500 Oe).

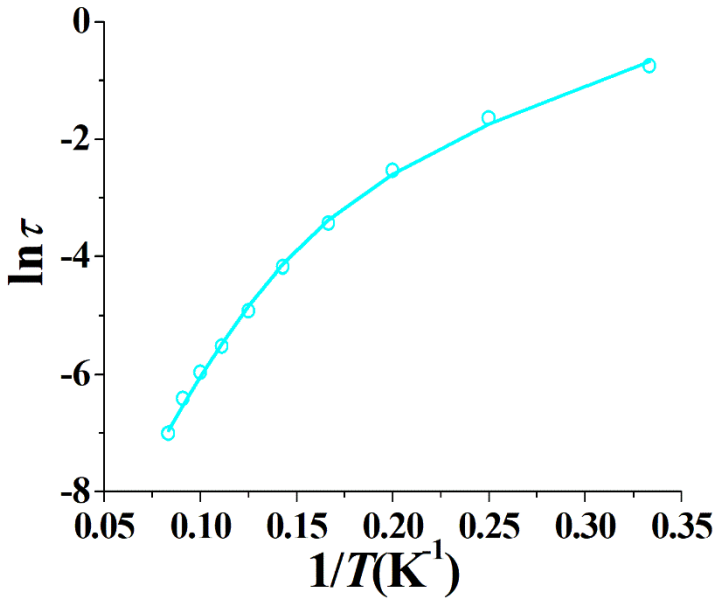

Fig. S8. Plot of ln(τ) *versus* 1/T for **1** (H_{dc} = 1500 Oe); the solid line represents the best fitting with Orbach *plus* Raman.

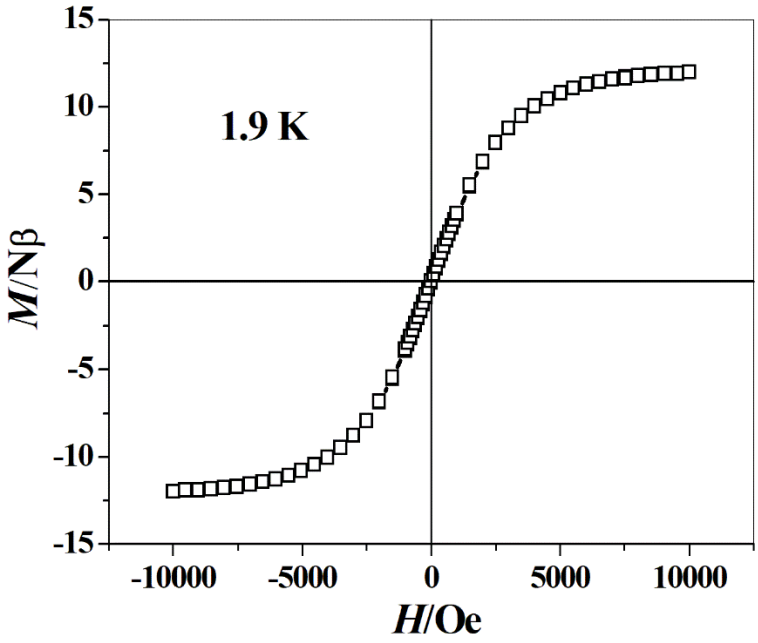

Fig. S9. Hysteresis loop for **2** at 1.9 K with the normal sweep rate (100-300 Oe min^{-1}).

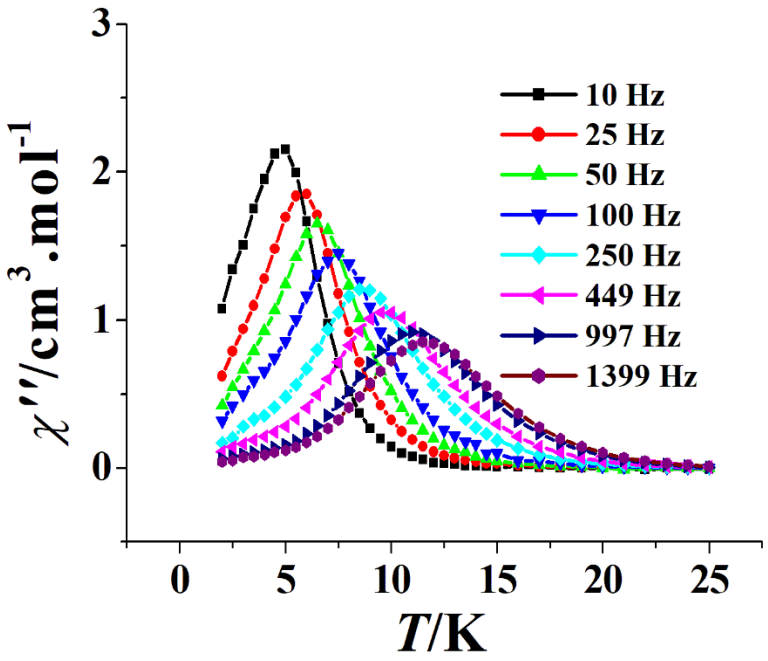

Fig. S10. Plots of χ'' *versus* T for **2** (H_{dc} = 1500 Oe).

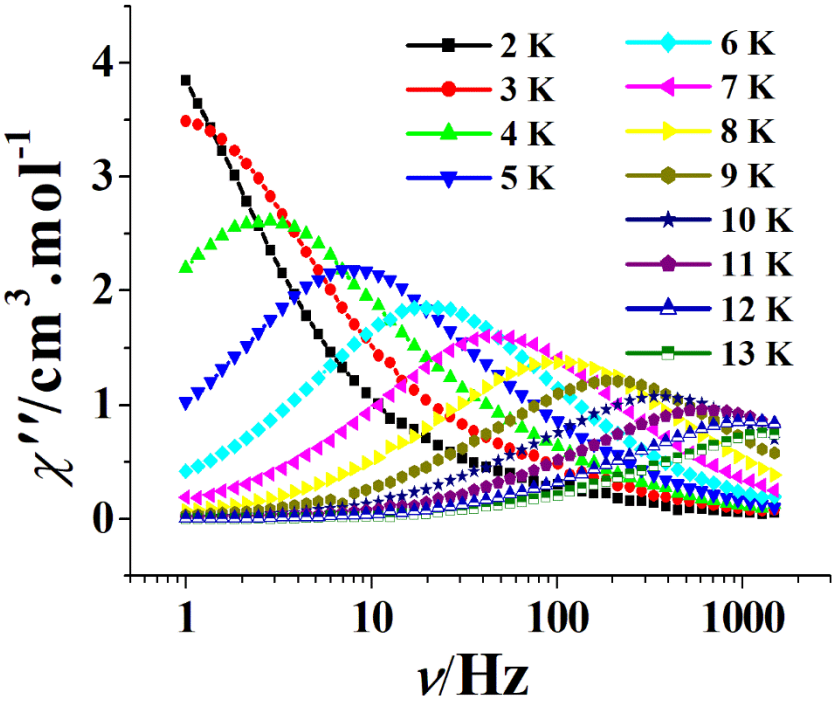

Fig. S11. Plots of χ'' *versus* ν for **2** (H_{dc} = 1500 Oe).

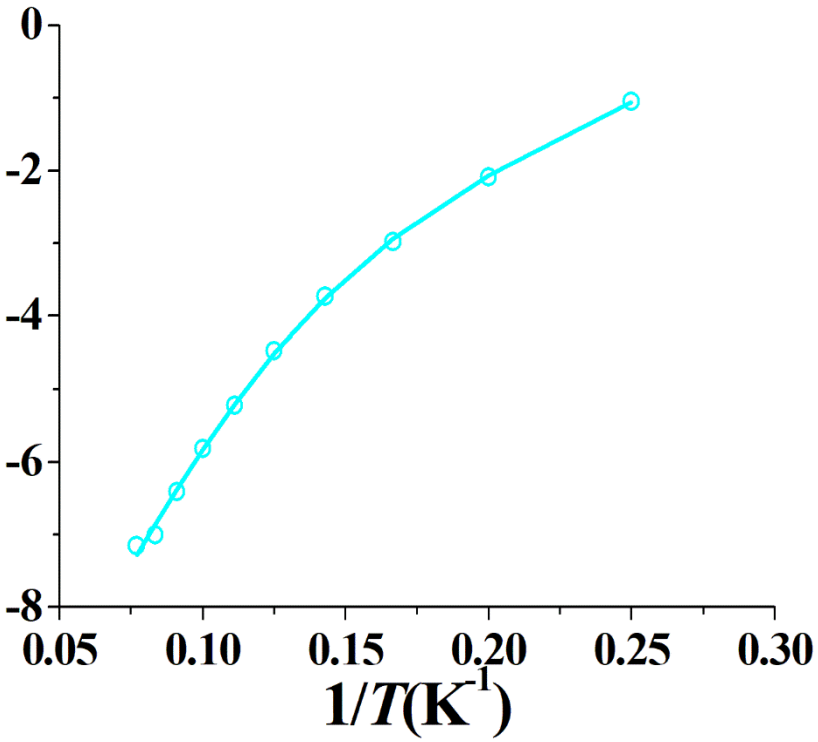

Fig. S12. Plot of ln(τ) *versus* 1/T for **2** (H_{dc} = 1500 Oe); the solid line represents the best fitting with Orbach *plus* Raman.

Computational details

For each of binuclear complexes **1** and **2**, we only need to calculate one individual Dy^{III} fragment (**1_Dy1** and **2_Dy1**, respectively) due to their centrosymmetric structures. Complete-active-space self-consistent field (CASSCF) calculations on individual Dy^{III} fragments for **1** and **2** (see Fig. S1 for the calculated complete structures of **1** and **2**) on the basis of single-crystal X-ray determined geometries have been carried out with the OpenMolcas[S1] program package. Each individual Dy^{III} fragment in **1** and **2** was calculated keeping the experimentally determined structure of the corresponding compound while replacing the neighboring Dy^{III} ion by diamagnetic Lu^{III}.

The basis sets for all atoms are atomic natural orbitals from the OpenMolcas[S1] ANO-RCC library: ANO-RCC-VTZP for Dy^{III}; VTZ for close N and O; VDZ for distant atoms. The calculations employed the second order Douglas-Kroll-Hess Hamiltonian, where scalar relativistic contractions were taken into account in the basis set and the spin-orbit couplings were handled separately in the restricted active space state interaction (RASSI-SO) procedure.[S2–S3] Active electrons in 7 active orbitals include all *f* electrons (CAS (9 in 7) in the CASSCF calculation. To exclude all the doubts, we calculated all the roots in the active space. We have mixed the maximum number of spin-free state which was possible with our hardware (all from 21 sextets, 128 from 224 quadruplets, 130 from 490 doublets for Dy^{III}. SINGLE_ANISO[S2] program was used to obtain the energy levels, ***g*** tensors, magnetic axes, *et al.* based on the above CASSCF/RASSI-SO calculations.

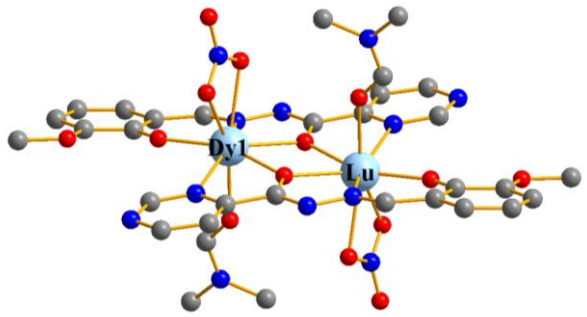

1_Dy1

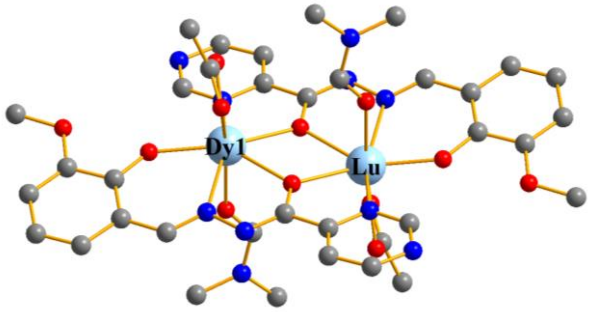

2_Dy1

Fig. S13. Calculated individual Dy^{III} fragments of **1** and **2**; H atoms are omitted for clarify.

Table S2. Calculated energy levels (cm^{-1}), ***g*** (g_x, g_y, g_z) tensors and predominant m_J values of the lowest eight Kramers doublets (KDs) of individual Dy^{III} fragments for **1** and **2** using CASSCF/RASSI-SO with the OpenMolcas.

KDs	**1_Dy1**			**2_Dy1**		
	E	***g***	m_J	*E*	***g***	m_J
0	0.0	0.007 0.012 19.637	±15/2	0.0	0.011 0.022 19.571	±15/2
1	211.2	0.133 0.165 16.999	±13/2	170.9	0.194 0.381 16.983	±13/2
2	385.8	3.195 6.061 10.367	-	269.8	0.443 1.244 17.030	-
3	425.9	0.071 3.376 12.996	-	328.1	1.223 2.725 13.897	-
4	441.8	3.634 3.833 10.432	-	349.7	1.097 2.116 10.712	-
5	532.4	9.828 6.563 3.029	-	425.0	4.433 5.652 10.139	-
6	563.4	1.641 3.929 14.443	-	454.9	2.184 2.848 14.239	-
7	577.1	0.563 5.609 11.326	-	538.8	0.153 0.269 19.034	-

Table S3. Wave functions with definite projection of the total moment | m_J > for the lowest eight KDs of individual Dy^{III} fragments for **1** and **2** using CASSCF/RASSI-SO with the OpenMolcas.

	E/cm^{-1}	wave functions
1_Dy1	0.0	96.0%|±15/2>
	211.2	82.7%|±13/2>+7.9%|±9/2>
	385.8	33.0%|±11/2>+26.7%|±1/2>+20.5%|±3/2>+5.5%|±13/2>+5.4%|±7/2>
	425.9	21.0%|±5/2>+20.6%|±1/2>+19.5%|±7/2>+15.5%|±11/2>+15.1%|±3/2>
	441.8	22.4%|±1/2>+19.9%|±3/2>+19.2%|±5/2>+16.7%|±11/2>+12.8%|±9/2>
	532.4	34.2%|±9/2>+20.1%|±11/2>+14.1%|±7/2>+11.9%|±3/2>+11.7%|±5/2>
	563.4	27.6%|±3/2>+25.5%|±5/2>+20.0%|±7/2>+14.0%|±1/2>+10.0%|±9/2>
	577.1	36.2%|±7/2>+26.9%|±9/2>+20.3%|±5/2>+9.4%|±1/2>
2_Dy1	0.0	94.9%|±15/2>
	170.9	71.9%|±13/2>+10.9%|±9/2>+10.7%|±11/2>
	269.8	43.7%|±1/2>+31.2%|±3/2>+10.5%|±5/2>+4.8%|±7/2>
	328.1	27.8%|±5/2>+19.6%|±1/2>+14.4%|±3/2>+13.0%|±7/2>+10.8%|±9/2>+9.3%|±11/2>
	349.7	29.3%|±11/2>+17.5%|±7/2>+16.7%|±13/2>+13.2%|±3/2>+11.0%|±9/2>+6.9%|±5/2>
	425.0	28.7%|±7/2>+24.4%|±11/2>+20.5%|±5/2>+13.8%|±9/2>+7.1%|±3/2>
	454.9	26.7%|±3/2>+20.8%|±1/2>+20.0%|±9/2>+19.7%|±5/2>+8.3%|±11/2>
	538.8	31.6%|±9/2>+29.7%|±7/2>+13.6%|±5/2>+9.4%|±11/2>+6.9%|±3/2>

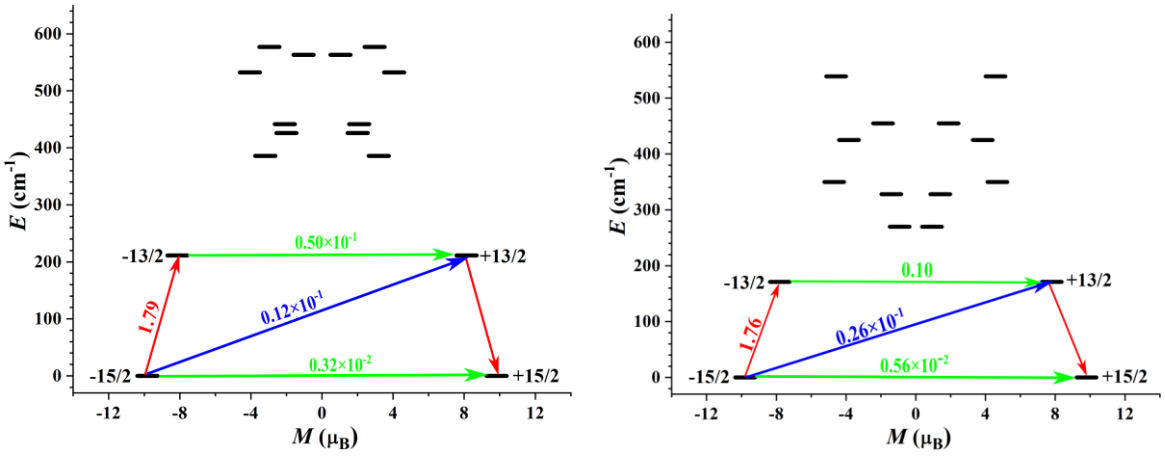

Fig. S14. Magnetization blocking barriers of individual Dy^{III} fragments for **1** and **2**. The thick black lines represent the KDs as a function of their magnetic moment along the magnetic axis. The green lines correspond to diagonal quantum tunneling of magnetization (QTM); the blue line represent off-diagonal relaxation process. The path shown by the red arrows represents the most probable path for magnetic relaxation in the corresponding compounds. The numbers at each arrow stand for the mean absolute value of the corresponding matrix element of transition magnetic moment.

To fit the exchange interactions in **1** and **2**, we took two steps to obtain them. Firstly, we calculated individual Dy^{III} fragments using CASSCF/RASSI-SO to obtain the corresponding magnetic properties. Then, the exchange interaction between the magnetic centers was considered within the Lines model,[S7] while the account of the dipole-dipole magnetic coupling was treated exactly. The Lines model is effective and has been successfully used widely in the research field of *d* and *f*-elements single-molecule magnets.[S8- S9]

For complexes **1** and **2**, there is only one type of $\tilde{J}$. The Ising exchange Hamiltonian is:

$$\hat{H}_{exch} = -\tilde{J}\,\hat{\tilde{S}}_{Dy1}\,\hat{\tilde{S}}_{Dy2} \tag{S1}$$

$\tilde{J} = 25\cos\varphi J$, where φ is the angle between the anisotropy axes on two Dy^{III} sites, and J is the Lines exchange coupling parameter. $\tilde{S}_{Dy} = 1/2$ is the ground pseudospin on the Dy^{III} site. $\tilde{J}_{total}$ is the parameter of the total magnetic interaction ($\tilde{J}_{total} = \tilde{J}_{dip} + \tilde{J}_{exch}$) between magnetic center ions. The dipolar magnetic coupling can be calculated exactly, while the exchange coupling constant was fitted through comparison of the computed and measured magnetic susceptibilities using the POLY_ANISO program.[S4-S6]

Table S4. Exchange energies E (cm^{-1}), the energy difference between each exchange doublets Δ_t (cm^{-1}) and the main values of the g_z for the lowest two exchange doublets of **1** and **2**.

	1			**2**		
	E	Δ_t	g_z	E	Δ_t	g_z
1	0.000000000000	8.091×10^{-7}	39.276	0.000000000000	3.199×10^{-6}	39.144
	0.000000809097			0.000003198535		
2	1.636012385591	1.529×10^{-6}	0.000	1.217504953395	5.096×10^{-6}	0.000
	1.636013915023			1.217510049869		

References:

S1 Galván, I. F.; Vacher, M.; Alavi, A.; Angeli, C.; Aquilante, F.; Autschbach, J.; Bao, J. J.; Bokarev, S. I.; Bogdanov, N. A.; Carlson, R. K.; Chibotaru, L. F.; Creutzberg, J.; Dattani, N.; Delcey, M. G.; Dong, S. S.; Dreuw, A.; Freitag, L.; Frutos, L. M.; Gagliardi, L.; Gendron, F.; Giussani, A.; González, L.; Grell, G.; Guo, M. Y.; Hoyer, C. E.; Johansson, M.; Keller, S.; Knecht, S.; Kovacevic, G.; Källman, E.; Manni, G. L.; Lundberg, M.; Ma, Y. J.; Mai, S.; Malhado, J. P.; Malmqvist, P. Å.; Marquetand, P.; Mewes, S. A.; Norell, J.; Olivucci, M.; Oppel, M.; Phung, Q. M.; Pierloot, K.; Plasser, F.; Reiher, M.; Sand, A. M.; Schapiro, I.; Sharma, P.; Stein, C. J.; Sørensen, L. K.; Truhlar, D. G.; Ugandi, M.; Ungur, L.; Valentini, A.; Vancoillie, S.; Veryazov, V.; Weser, O.; Wesołowski, T. A.; Widmark, Per-Olof.; Wouters, S.; Zech, A.; Zobel, J. P.; Lindh. R. *J. Chem. Theory Comput.* **2019**, *15*, 5925–5964.

S2 Malmqvist, P. Å.; Roos, B. O.; Schimmelpfennig, B. *Chem. Phys. Lett.,* **2002**, *357,* 230–240.

S3 Heß, B. A.; Marian, C. M.; Wahlgren, U.; Gropen, O. *Chem. Phys. Lett.,* **1996**, *251,* 365–371.

S4 Chibotaru, L. F.; Ungur, L.; Soncini, A. *Angew. Chem., Int. Ed*. **2008**, *47*, 4126–4129.

S5 Ungur, L.; Van den Heuvel, W.; Chibotaru, L. F. *New J. Chem.* **2009**, *33*, 1224–1230.

S6 Chibotaru, L. F.; Ungur, L.; Aronica, C.; Elmoll, H.; Pilet, G.; Luneau, D. *J. Am. Chem. Soc*. **2008**, *130*, 12445–12455.

S7 Lines, M. E. *J. Chem. Phys*. **1971**, *55*, 2977−2984.

S8 Mondal, K. C.; Sundt, A.; Lan, Y. H.; Kostakis, G. E.; Waldmann, O.; Ungur, L.; Chibotaru, L. F.; Anson, C. E.; Powell, A. K. *Angew. Chem., Int. Ed.* **2012**, *51*, 7550−7554.

S9 Langley, S. K.; Wielechowski, D. P.; Vieru, V.; Chilton, N. F.; Moubaraki, B.; Abrahams, B. F.; Chibotaru, L. F.; Murray, K. S. *Angew. Chem., Int. Ed.* **2013**, *52*, 12014–12019.